

Threshold-based prediction of the coagulation zone in sequential temperature mapping in MR-guided radiofrequency ablation of liver tumours

Hansjörg Rempp · Rüdiger Hoffmann · Jörg Roland ·
Alexandra Buck · Antje Kickhefel · Claus D. Claussen ·
Philippe L. Pereira · Fritz Schick · Stephan Clasen

Received: 14 July 2011 / Revised: 15 September 2011 / Accepted: 27 September 2011 / Published online: 22 November 2011
© European Society of Radiology 2011

Abstract

Objective To evaluate different cut-off temperature levels for a threshold-based prediction of the coagulation zone in magnetic resonance (MR)-guided radiofrequency (RF) ablation of liver tumours.

Methods Temperature-sensitive measurements were acquired during RF ablation of 24 patients with primary (6) and secondary liver lesions (18) using a wide-bore 1.5 T MR system and compared with the post-interventional coagulation zone. Temperature measurements using the proton resonance frequency shift method were performed directly subsequent to energy application. The temperature maps were registered on the contrast-enhanced follow-up MR images acquired 4 weeks after treatment. Areas with temperatures above 50°, 55° and 60°C were segmented and compared with the coagulation zones. Sensitivity and positive predictive value were calculated.

Results No major complications occurred and all tumours were completely treated. No tumour recurrence was observed at the follow-up examination after 4 weeks. Two patients with secondary liver lesions showed local tumour recurrence after 4 and 7 months. The 60°C threshold level achieved the highest positive predictive value (87.7 ± 9.9) and the best prediction of the coagulation zone.

Conclusions For a threshold-based prediction of the coagulation zone, the 60°C cut-off level achieved the best prediction of the coagulation zone among the tested levels.

Key Points

- Temperature monitoring can be used to survey MR-guided radiofrequency ablation
- The developing ablation zone can be estimated based on post-interventional temperature measurements
- A 60°C threshold level can be used to predict the ablation zone
- The 50°C and 55°C temperature zones tend to overestimate the ablation zone

H. Rempp (✉) · R. Hoffmann · A. Buck · C. D. Claussen ·
F. Schick · S. Clasen
Department on Diagnostic and Interventional Radiology,
Eberhard Karls University of Tübingen,
Hoppe-Seyler-Straße 3,
72076 Tübingen, Germany
e-mail: Hansjoerg.rempp@med.uni-tuebingen.de

J. Roland · A. Kickhefel
Siemens Healthcare,
Henkelstraße 197,
91054 Erlangen, Germany

P. L. Pereira
Clinic for radiology, Nuclear Medicine and Minimal Invasive
Therapies, SLK-Clinics,
Am Gesundbrunnen 20-26,
74078 Heilbronn, Germany

Keywords Radiofrequency ablation · Magnetic resonance imaging · Proton resonance frequency shift method · Interventional procedures · MR thermometry

Introduction

Percutaneous radiofrequency (RF) ablation is an increasingly accepted therapy option for primary and inoperable secondary liver tumours [1–4]. Small wounds, a short hospitalisation of the patients and a relatively low morbidity and mortality rate are some of the advantages of this local treatment strategy [5]. However, especially for larger

tumours, local recurrence is still a problem and recurrence rates are higher than in comparable patient groups which underwent surgical treatment, depending on the tumour size [6–8]. This may be due to the limited ability of most RF systems to achieve large coagulation zones, especially orthogonally to the applicator axis [9]. In addition, ultrasound and CT-guidance, commonly used for therapy monitoring in the percutaneous approach, have limited capacities to visualise the developing ablation zone [8, 10]. In comparison to other imaging techniques, MR temperature mapping allows direct visualisation of the physical effect underlying the tissue modifications caused by applying energy. The proton resonance frequency shift method calculates relative temperature changes between phase images acquired at different moments [11]. Thermal dose mapping based on a continuous acquisition of temperature data during energy application is the most elaborated technique for therapy monitoring and offers the almost immediate visualisation of the temperature of each voxel [12, 13]. Sequential temperature mapping is the acquisition of singular, and if necessary, repeated temperature maps subsequent to energy application side-stepping the necessity of filtering the RF which otherwise interferes with the measurements [14]. The direct benefit of the temperature maps is the potential for the protection of sensitive anatomical structures adjacent to the target lesion and the visualisation of a possible heatsink effect caused by vessels crossing the tumour. Furthermore, temperature maps can be used to estimate the size and location of the developing coagulation zone [14]. The objective of this work was to compare the temperature maps generated at the end of thermal therapy using the proton resonance frequency shift method (PRF) with the coagulation zones and to evaluate different cutoff temperature values with regard to their ability to correctly predict the ablation zone.

Materials and methods

Patients

The institutional review board approved MR-guided treatment of the patients. The decision in favour of therapy was made by the institutional interdisciplinary tumour board conference. Informed consent was given by all patients. Twenty-four patients, 17 men and 7 women were treated using MR-guided RF ablation. The mean patient age was 66 years, and patient age ranged between 39 and 82 years. Six patients suffered from a hepatocellular carcinoma, 18 from liver metastases of non-hepatic primary cancers. Among them, 11 patients had a colon carcinoma, 6 suffered from melanoma and one from non-small cell lung cancer.

Mean lesion size was 23 ± 9 mm; the lesion size ranged from 8 mm to 52 mm (median 20 mm, interquartile range 11 mm).

Radiofrequency ablation

All ablation therapies were performed using a wide-bore 1.5 T MR system (Magnetom Espree, Siemens Healthcare, Erlangen, Germany). Patients were positioned supine with feet forward. A six-channel body array and an additional loop array were used. All patients were treated under analgesic sedation using midazolom (up to 7 mg) and piritramid (up to 15 mg) intravenously. Before starting the treatment, a planning examination was performed using standard MR sequences including T2-weighted coronal half-fourier acquisition single-shot turbo spin-echo (HASTE) sequences and T2-weighted transversal turbo spin-echo sequences. Additionally, a transverse T1-weighted fast spin-echo sequence was performed. Patients with hepatocellular carcinoma also underwent a gadolinium-based contrast-enhanced dynamic liver examination (see below for details). An internally water-cooled bipolar MR-compatible RF system was used for therapy (Olympus Celon, Teltow, Germany).

Depending on the tumour size, two applicators with a length of the active tip of 3 cm (in 13 patients) or 4 cm (in 11 patients) were used. The applicators were placed under the guidance of fluoroscopic sequences which allowed the parallel display of three different slice angulations. When both applicators were placed in the target tissue, energy application was started. Energy was applied in multipolar mode by a RF generator, meaning the high frequency electric field was placed between the two applicators. The power settings were chosen according to the recommendations of the manufacturer; maximal initial power output was between 45 and 55 watts, adapted to the tumour location and patients' well-being. Energy application was performed in steps of 30 kJ and was followed by temperature-sensitive measurements. Application was stopped when the mean power output indicated by the RF generator had decreased below 20 watts. Mean energy application was 139 ± 24 kJ. During energy application, both applicators were internally water-cooled using a flow of 100 ml/min. Temperature maps were acquired directly subsequent to energy application. T1-weighted images were acquired and the energy application was continued if the T1 hyperintense safety margin was below 5 mm or if T1 hypointense residual tumour tissue was detected. Therapy decision was based on T1-weighted images. In the case of remaining tumour tissue which could not be reached by the first applicator position, the probes were repositioned and another therapy cycle was started.

MR sequences

a) Temperature mapping

The PRF method was used for temperature mapping [15]. A segmented gradient echo RF-spoiled free induction decay echo planar imaging (EPI) sequence was used to acquire phase images. Image parameters included: repetition time (TR)=800 msec, echo time (TE)=8 msec, field of view (FOV)=256×256, resolution=128×128, flip angle=25°, bandwidth 400 Hz/pixel, slice thickness=2 mm. Acquisition time for three slices was 3.3 s. The pixel size was 2×2 mm². Fat saturation was implemented, and at least three slices were acquired. An abdominal breathing belt was used for image gating on the respiration cycle to minimise motion artefacts. Image acquisition was performed in late expiration phase during a time window of 0.8–1.2 s. Phase images were acquired directly before starting the therapy (serving as a baseline image) and repeatedly after the application of 30 kJ. Energy application was continued in the case of remaining tumour tissue, and temperature mapping was repeated after further application of 30 kJ or if the power output decreased below 20 watts. Mean number of temperature measurements per patient was 5 (range 3–8). The detected phase changes between the measurements and the baseline images were proportional to temperature changes in the respective tissue and served to calculate voxel-specific temperature changes [16]. A phase drift was detected by a 5×5 pixel detection window placed on a region in the liver where no temperature changes were expected. A software-based subtraction of the detected phase differences was performed before calculating the temperature changes. An imaging plane containing both RF applicators was measured; a second plane was orthogonal to the applicators, crossing them at the centre of the active tips. The third imaging plane was placed between the applicators and was orthogonal to the other planes. Temperature maps were directly calculated and displayed by a colour-encoded map overlaying the anatomical magnitude image using the integrated imaging software. In case of repeated temperature measurements in one patient, the measurement with the largest expansion of the heated zone was selected.

b) Follow-up examination

All patients underwent an MR follow-up examination at 1.5 T (Siemens Avanto, Siemens Healthcare, Erlangen, Germany) 4 weeks after therapy and subsequently every 3 months during the first year. The examination included standard MR sequences [14, 17, 18], including a T2-weighted coronal HASTE sequence, a T2-weighted transversal turbo spin-echo sequence, a diffusion-weighted transversal echo planar imaging sequence and a non-enhanced T1-weighted transversal fast low angle shot

gradient echo (FLASH) sequence. A 3D-encoded FLASH sequence was part of the protocol for a contrast-enhanced dynamic liver study after intravenous injection of macrocyclic gadobutrol (Gadovist, Bayer Healthcare, Leverkusen, Germany; dose: body weight/10 mL of gadobutrol, corresponding to 0.1 mmol/kg at an injection rate of 2 mL/s followed by 20 mL of normal saline solution) with the parameters: TR=3.19 msec, TE=1.49 msec, slice thickness=2 mm, resolution 256×200, bandwidth=560 Hz/pixel, flip angle=10°, number of slabs=2, number of slices per slab=88; the number of slices per slab were adapted to the individual patient. Images were acquired before and 20, 40 and 60 s after applying a contrast agent.

Data analysis

The follow-up-examination after 4 weeks served as a gold standard for the size and localisation of the coagulation zone. This examination was chosen because the initial images directly after therapy were often of lower quality due to sedation-related breathing artefacts; furthermore, the coagulation zone tends to increase during the first week post-intervention in some patients. For optimal detection of the coagulation zone, the datasets of the portal-venous phase images from the contrast-enhanced dynamic liver examination were loaded to a 3D visualisation software (Syngo.via, Siemens Healthcare, Erlangen, Germany) and the patient-specific slice orientation of the temperature maps was reproduced by the interventionalist based on the angulation information of the slices and anatomical landmarks within the liver such as vessel bifurcations [19]. The selected slices of the dynamic liver examination were registered on the magnitude images of the temperature maps using software programmed based on the Matlab non-rigid image registration tool (Image processing toolbox, MatLab, V. 7.1, MathWorks, Natick, MA, USA). At least five anatomical image features within the liver such as vessel bifurcations which served as matching points were selected on the corresponding images before a multivariate image transformation was performed. Images were cut and automatically resized. Using this dataset, the non-enhancing liver parenchyma, which corresponds to the coagulation zone, was manually segmented by a radiologist following the inner border of the surrounding rim of enhancing tissue. This area was compared (1) to the segmented areas with a displayed temperature above 50°C, (2) above 55°C and (3) above 60°C. During the segmentation of the temperature maps, only voxels in direct contact with the displayed heated area were included into the segmented area, that is, one contiguous zone was segmented and presumably erroneous singular voxels with above threshold temperatures in the periphery were omitted (see Fig. 3b and d). If various sequential temperature measurements with identical

applicator positions were available, the temperature map with the largest geometrical expansion, that is, the time-point with the largest area segmented, was selected. If two sequential ablation cycles with different applicator positions were performed, all heated areas in both temperature maps were segmented, fused and compared with the contrast-enhanced imaging. Matching points between the segmented temperature area and the non-enhancing area were referred to as true positive. Segmented areas in the temperature map which did not correspond to the non-enhancing zone were referred to as false positive. Non-enhancing voxels without correspondence on the temperature map were regarded as false negative. Sensitivity was calculated as true positive / (true positive + false negative) and represents the portion of the coagulation zone which was correctly predicted by the temperature map. Positive predictive value was calculated as true positive / (true positive + false positive) and represents the portion of the area in the temperature map above the selected cutoff value that correctly detected the coagulation zone. Enhancing voxels below the temperature threshold were regarded as true negative. Negative predic-

tive value was calculated as true negative / (true negative + false negative) and describes the portion of voxels below the threshold that remained vital. Specificity was calculated as true negative / (true negative + false positive) and represents the portion of the vital liver parenchyma which was correctly predicted to remain non-coagulated.

The surface of the segmented area in the temperature map and the surface of the segmented coagulation zone were compared and the ratio between them was calculated. The largest diameter of the coagulation zone and of the segmented temperature area was measured. The quality of image registration was estimated based on the liver outline in the temperature maps and the corresponding selected contrast-enhanced image slices. The liver outlines were segmented and an index QI which described the proportion of the number of pixels included in both segmented areas (matching pixels) and the number of all segmented pixels was calculated: $QI = \text{number of matching pixels} / \text{number of all segmented pixels}$. Temperature maps with a QI below 0.90 were excluded from the evaluation. Diagnostic quality of the temperature maps was considered insufficient if a clear differentiation of the

Table 1 Patient data including age, sex, tumour histology, -location and -size. Two local tumour recurrences (Lp) appeared 4 and 7 months after therapy. (F female, M male, HCC hepatocellular carcinoma, metastasis of colorectal, melanoma and lung cancer, Lp Local tumour progression)

Patient	Patient age	Patient sex	Primary tumour	Liver segment	Tumour size (mm)	Coagulation zone size (mm)	Applied energy (kJ)	Follow up (months)
1	64	F	Colorectal	VIII	21×18	45×40	160	13
2	60	M	Colorectal	III	24×18	42×24	145	10
3	77	M	HCC	V	33×30	34×31	145	13
4	82	M	Colorectal	VI	19×17	37×21	140	13
5	69	F	HCC	III	18×13	38×38	115	10
6	76	M	HCC	VIII	26×23	37×37	145	10
7	39	M	Melanoma	IVa	37×28	44×36	180	13
8	70	F	HCC	VI	25×15	39×37	128	10
9	60	F	Melanoma	VI	8×8	47×28	90	19
10	55	F	Melanoma	V	18×14	44×27	112	10
11	69	M	HCC	IVb	52×52	60×56	195	13
12	66	M	Colorectal	VII	14×13	38×20	106	13
13	47	M	Colorectal	VI	18×17	54×26	145	13
14	72	M	Lung CA	VIII	30×26	53×27	160	Lp (4)
15	81	M	Colorectal	IVa	19×12	42×24	110	13
16	55	M	Colorectal	VIII	19×15	36×36	140	10
17	73	M	Colorectal	III	30×27	58×41	157	10
18	79	M	Colorectal	VII	29×22	54×30	155	13
19	79	M	HCC	VI	16×16	60×51	144	13
20	64	F	Melanoma	VIII	9×9	33×17	100	13
21	55	F	Melanoma	VIII	27×21	38×36	150	10
22	68	M	Colorectal	IV	29×21	56×34	155	Lp (7)
23	57	M	Melanoma	III	18×13	38×27	130	13
24	68	M	Colorectal	VI	18×15	43×34	135	10

temperature zones was impeded by phase inconsistencies. The accuracy of temperature mapping was estimated by calculating the standard deviation (SD) of temperature measurements in a non-heated area of the liver based on a region of interest comprising 100 pixels. If the treated area was in the left liver lobe, a non-heated area was selected in segment V or VIII; for treated areas in the right liver lobe, non-heated areas in the left liver lobe were observed. Signal-to-noise ratio (SNR) was determined for the portal-venous phase of the contrast-enhanced liver examination and for the magnitude images of the temperature maps and was calculated as signal in the liver parenchyma divided by the SD of the background noise. Average signal values of a spheric region of interest containing 12 pixels were used. Contrast-to-noise ratio (CNR) was calculated as the difference between the signal of the coagulation zone and healthy liver parenchyma divided by the SD of the background noise.

Statistical analysis

A Mann-U Whitney Test was used to compare the sensitivity and positive predictive value of the three different temperature cutoff values (50°C, 55°C and 60°C).

Results

All ablation therapies were technically successful (24/24). Minor complications occurred in 5/24 patients (21%); all five developed self-limiting subcapsular hematomas which did not require therapy. Major complications were not observed. Two local tumour recurrences (2/24; 8%) were observed after 4 and 7 months, one in a 72-year-old male patient with liver metastasis of non-small cell lung cancer, another in a 68-year-old male patient with a singular hepatic metastasis of a colorectal carcinoma. The metastases were 29 and 30 mm in size and the safety margins were judged narrow on the day of treatment and in the first controls, based on the non-enhanced T1-weighted images and the contrast-enhanced dynamic liver examination. In one of the cases, temperature mapping was not of diagnostic quality, in a second, the slice of the temperature map did not cover the concerned area. Both cases were successfully retreated using RF ablation. The mean follow-up period was 12 ± 2 months. Patient characteristics are summarised in Table 1.

Among the acquired temperature-sensitive measurements, a set of three differently angulated images acquired at same moment was selected for every patient (24

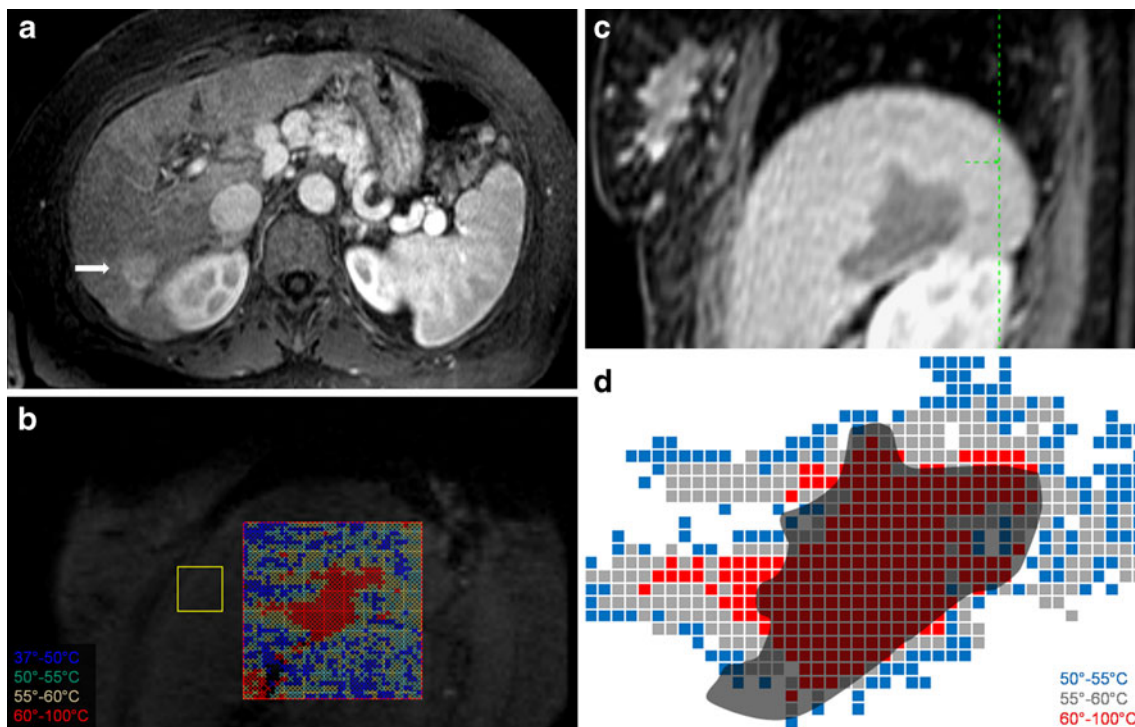


Fig. 1 **a** Pre-interventional imaging of a 70-year-old female patient with arterialised HCC lesion (*arrow*) in liver segment VI (patient number 8). **b** Sagittal oblique angulated temperature map with red encoded temperatures above 60°C, yellow encoded temperatures above 55°C and green encoded temperatures above 50°C. The measurements were directly acquired after energy application. **c** Contrast-enhanced dynamic liver examination 4 weeks after therapy with sagittal oblique slice angulation. The non-enhancing area

corresponds to the coagulation zone. **d** Result of the image registration and segmentation. The red encoded area corresponds to voxels with a temperature above 60°C, the grey encoded to a temperature above 55°C and the blue encoded to temperatures above 50°C. The dark grey area corresponds to the non-enhancing coagulation zone in the MR follow-up examination. Only heated voxels with direct contact to the coagulation zone were included by the segmentation

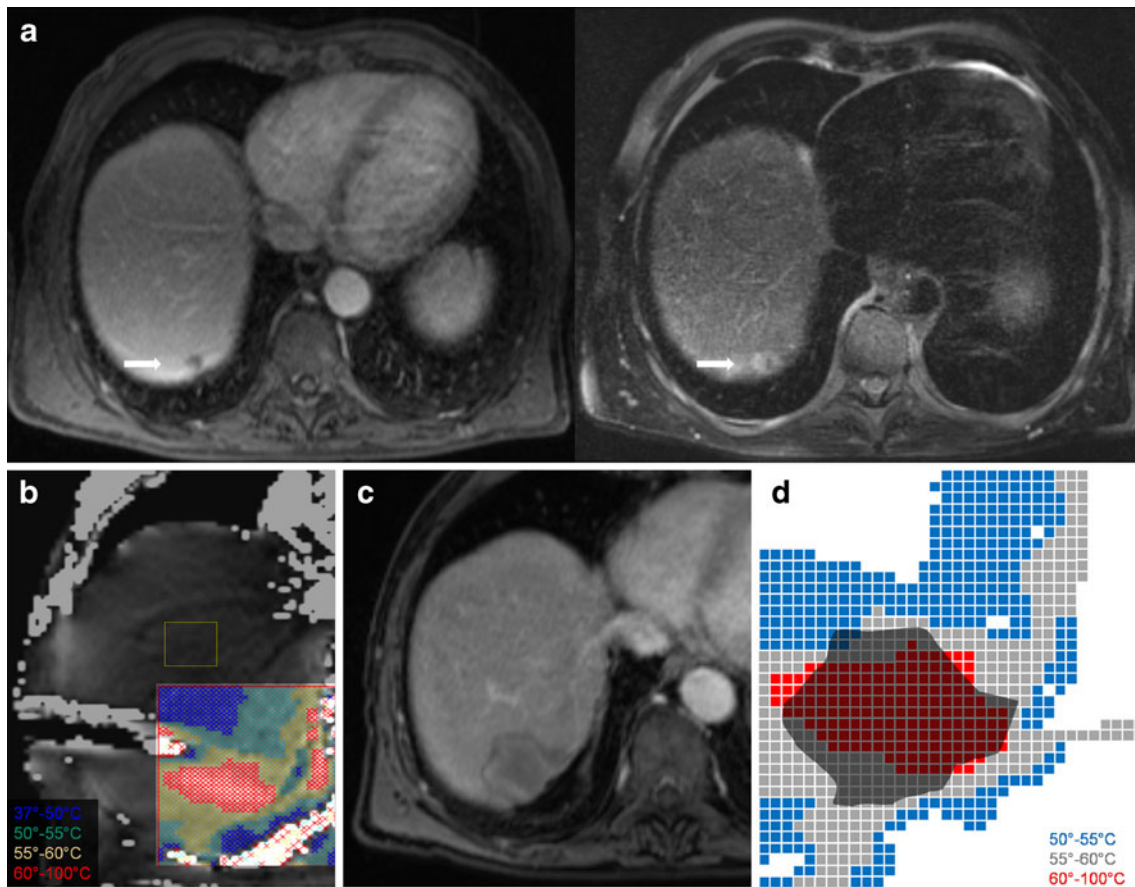


Fig. 2 **a** 66-year-old male patient with subcapsular metastasis (arrows) of colorectal cancer in liver segment VII (patient number 12). Contrast-enhanced image (left) and T2-weighted image (right). **b**

Temperature map **c** Contrast-enhanced follow-up image **d** Results of registration and segmentation of the different threshold temperature levels

patients \times 3=72 temperature maps) which represented the largest temperature expansion, i.e. the peak temperature. Nine measurements were not of diagnostic quality, and temperature map image registration and segmentation for an additional two were not of sufficient quality and thus were not evaluated. The remaining 61 temperature maps were evaluated (61/72). Examples of the treated lesions, the acquired temperature maps, the coagulation zones and the resulting image segmentation and evaluation are given in Figs. 1, 2 and 3.

Sensitivity describes the portion of the coagulation zone in the contrast-enhanced images which corresponded in the temperature maps to areas with a temperature above the selected temperature cut-off value. With decreasing cut-off values, this portion increased. Sensitivity was $81.0\pm 12.0\%$ for the 60°C -temperature zone. It increased to $84.5\pm 12.0\%$ at the 55°C -temperature zone and reached $88.7\pm 12.1\%$ at the 50°C temperature zone. The differences between the 50°C and the 60°C temperature zones were significant ($P=0.0002$), as were the differences between the 50°C and the 55°C temperature zones ($P=0.005$). Sensitivity and positive

predictive value are summarised in Table 2, the results of the statistical tests in Table 3.

The positive predictive value describes the portion of the area with a temperature above the selected cut-off value that correctly reflected the coagulation zone. The predictability of the coagulation zone based on the temperature maps increased with rising cut-off temperature values. The positive predictive value was $71.3\pm 16.0\%$ for the 50°C temperature zone. This increased to $74.5\pm 12.4\%$ at the 55°C temperature zone and reached $87.7\pm 9.9\%$ at the 60°C temperature zone. The differences of the positive predictive values between the tested temperature zones were significant (see Table 3). The positive predictive value for the area with temperatures between 50°C and 60°C was $23.5\pm 17.3\%$; for the subgroup with temperatures between 60°C and 55°C $34.4\pm 16.2\%$ and for the area with temperatures between 55°C and 50°C $17.0\pm 12.5\%$.

Specificity describes which portion of the non-coagulated liver parenchyma was correctly predicted to remain vital. Specificity was $96\pm 3.1\%$ for the 50°C

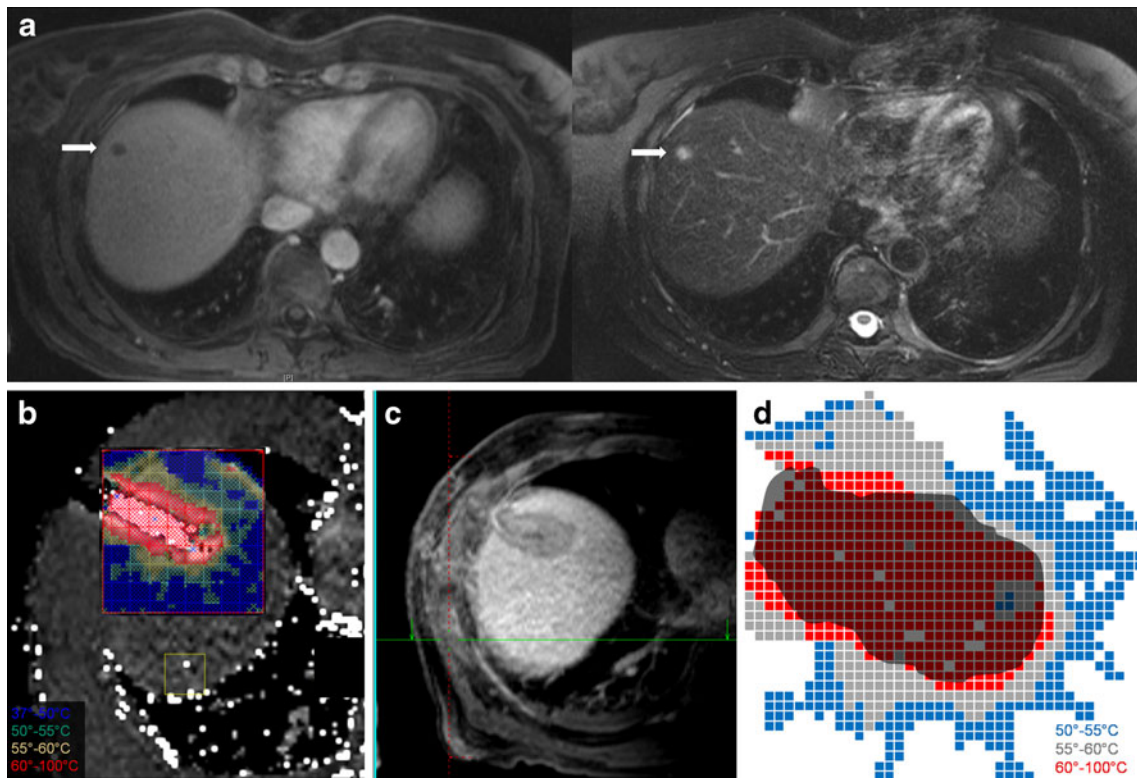


Fig. 3 a 64-year-old female patient with metastatic melanoma in liver segment VIII (arrows, patient number 20). Pre-interventional contrast-enhanced image (left) Pre-interventional T2-weighted image (right). b

Temperature map, c Contrast-enhanced follow-up imaging and d results of the registration and segmentation

temperature zone, $97 \pm 2.6\%$ for the 55°C and $99 \pm 2.1\%$ for the 60°C temperature zone.

The negative predictive value defines the portion of the area below the temperature threshold which truly remained vital. The negative predictive value was $99 \pm 1.2\%$ for the 50°C threshold, $98 \pm 2.3\%$ for the 55°C -threshold and $97 \pm 2.9\%$ for the 60°C -threshold.

The quality of registration influences the calculation of sensitivity and positive predictive value. The quality of image registration was evaluated by the factor QI, which describes the ratio between the matching and the non-matching liver areas on the registered images. Mean QI was

0.92 ± 0.04 . Due to distortions, two temperature maps could not be adequately registered and were excluded from the evaluation.

Signal-to-noise ratio in the portal venous phase of the contrast-enhanced FLASH-sequence was 91.2 ± 24.7 for the liver parenchyma and 58.1 ± 16.8 for the coagulation zone. Mean contrast-to-noise ratio between the liver and the coagulation zone was 33.1 ± 15.9 . SNR of the liver parenchyma was 54 ± 11.2 for the EPI sequence. The standard deviation for the temperature measurements in non-heated areas of the liver ranged between 1.0 and 3.9°C . The absolute highest temperature measured for a single pixel was 97.8°C , the mean highest temperature per patient was $92.1 \pm 3.8^\circ\text{C}$.

The ratio between the area segmented in the temperature map and the segmented coagulation zone was different for the selected cut-off temperatures. This ratio is independent from image misregistration. The ratio between the temperature area above 50°C and the coagulation zone was 1.32 ± 0.38 . This decreased to 1.15 ± 0.27 at the 55°C temperature zone and reached 0.96 ± 0.13 at 60°C . The area with a temperature of 50°C or above was thus in mean 32% larger than the coagulation zone, with a large standard deviation of $\pm 38\%$, based on the evaluation of 61 temperature maps.

Table 2 Sensitivities and positive prospective values of temperature maps at different cut-off temperatures for the prediction of the coagulation zone

Cut-off temperature (°C)	Sensitivity (n=61) mean ± SD in percent	Positive prospective value (n=61) mean ± SD in percent
50	88.7 ± 12.1	71.3 ± 16.0
55	84.5 ± 12.0	74.5 ± 12.4
60	81.0 ± 12.0	87.7 ± 9.9

Table 3 *P*-values for the statistic analysis between the different cut-off temperature zones using the Mann–Whitney-U-Test

Cut-off temperature zone (°C)	Sensitivity	Positive prospective value
50–55	<i>P</i> =0.00498	<i>P</i> =0.04083
55–60	<i>P</i> =0.13753	<i>P</i> =6.1×10 ⁻⁸
50–60	<i>P</i> =0.00021	<i>P</i> =8.14×10 ⁻⁹

The area with a temperature of 55°C or above was 15±27% larger than the coagulation zone. The area with a temperature of 60°C or above was 4±13% smaller than the coagulation zone. The largest mean diameter of the segmented temperature area was 53.2±11.4 mm at the 50°C threshold and decreased to 45.6±8.22 mm at the 60°C threshold. The largest mean diameter of the coagulation zone was 44.6±8.4 mm on contrast-enhanced imaging after 4 weeks. An overview of the ratios and diameters is given in Table 4.

Discussion

Feasibility of MR temperature mapping during MR-guided interventions has been shown in different studies with a small number of patients and PRF-based temperature mapping techniques [13, 17]. While the precision of the acquired temperature data is difficult to evaluate during thermoablative therapy due to the high local temperature differences around the applicator, overall accuracy of the measurements was investigated and has been shown to be acceptable for therapy monitoring, if fast sequences and breathing gating techniques are applied [16, 20, 21]. Temperature mapping can be used to protect sensitive structures in the vicinity of the targeted tumours from heat damage. Furthermore, it may be useful to determine the therapy endpoint. The continuous acquisition of temperature data during energy application allows the calculation of thermal dose maps. Based on this voxel-specific data, the development of necrosis can be predicted, although the direct correlation between the thermal dose and the ablation zone in the follow-up has not been proven yet [12, 22]. This

approach, however, necessitates filtering the RF waves and a continuously acquiring MR temperature maps during therapy. With temperature map acquisitions at selected moments in pauses of energy application, no filtering of the RF waves is necessary. Sequential temperature mapping as well as thermal dose maps can be used to estimate the extension and location of the developing coagulation zone [23]. In vivo studies reported a temperature level of 51°C or 52°C for a threshold-based prediction of cell death [23–25]. In our data, the use of different temperature cut-off levels resulted in different levels of sensitivity and positive predictive value in the prediction of the coagulation zone. Sensitivity of the temperature maps decreased for higher temperature cut-off levels, whereas positive predictive values increased with rising cutoff temperature levels. This agrees with our expectations, due to the increased probability of high temperatures being located in the centre of the ablation zone. For clinical practice, a high positive predictive value of the temperature maps is necessary, as therapy monitoring based on false positive results in the temperature maps may cause remaining local tumour tissue to be overlooked. We demonstrated that a cut-off temperature level of 60°C achieved the most accurate estimation of the area of the coagulation zone. A threshold level of 50°C and 55°C led to an overestimation of the coagulation zone and are therefore less adequate as predictive factors. A major limitation of this binary interpretation of temperature mapping is its low temporal resolution. The induction of tissue necrosis does not only depend on the actual tissue temperature reached during energy application but also on the duration of elevated tissue temperatures, which can already lead to necrosis in the temperature range between 43–52°C, if the duration of the temperature elevation is sufficiently long. This fact is optimally taken into consideration by thermal dose maps, calculating the accumulated temperature dose per voxel [13, 17, 26]. From the present data, it can be concluded that the underestimation of the developing coagulation zone in areas with sub-threshold temperatures is not a major problem of sequential temperature mapping. The majority of voxels with a temperature of 50°C and 55°C did not match the coagulation zone in the registered images; this is reflected by the relatively low

Table 4 Characteristics of the coagulation zones and segmented areas on the temperature maps (TMap) at different cut-off temperatures. Largest diameters of the areas and the ratio between the segmented areas and the coagulation zones are given

Cut-off temperature (°C)	Largest tumour diameter (mm, mean±SD)	Largest coagulation zone diameter (mm, mean±SD)	Largest diameter segmented area in TMap (mm, <i>n</i> =61)	Ratio between segmented areas: TMap/Coagulation zone
50	23.2±9.3	44.6±8.4	53.2±11.4	1.32±0.38
55			48.8±9.01	1.15±0.27
60			45.6±8.22	0.96±0.13

positive predictive values for this area. Temperature maps and the significant differences between the positive predictive values of the temperature cut-off levels support the assumption of a zonal configuration of the temperature levels around the electrodes. For some of the peripheral voxels it can be proposed that they experienced temperatures above 50°C over several minutes, however they did not form part of the ablation zone. Comparison to other published data shows that the thermal dose maps may also tend to overestimate the coagulation zones at least in their short axis dimension [17]. It can be proposed that the slow progression of temperatures into the lethal range at the edge of the ablation zone allows cellular protection mechanisms such as heat shock proteins to be activated, limiting the necrosis to a core area of temperatures greater than at least 55°C [27, 28].

The high negative predictive values proved that the tested temperature thresholds may be useful for the protection of tissue at risk. As expected, the 50°C threshold achieved the best negative predictive value.

Different sources of errors interfering with our data have to be distinguished. A major problem is imprecision induced by the non-rigid registration of two data-sets acquired at different moments. Distortions and translational shifts of the images lead to non-systematic errors. In patients with subcapsular hematomas additional distortions may have influenced the evaluation. Furthermore, there is a potential bias based upon the time-point of post-interventional imaging. A change of the coagulation zones' diameters during the 4 weeks after therapy may influence the results. Different studies described a growth of the coagulation zone within the first week post intervention [29–31]; however, to our knowledge the post-interventional development of the coagulation zones' diameters in MR imaging has not been systematically analyzed yet. During the temperature measurements, a major source of error is patient interscan motion and artefacts induced by irregular breathing, misregistration of the breathing cycle and susceptibility artefacts of the RF applicators. The variability of the PRF temperature measurements may have led to a misclassification of data within the 5°C-temperature steps analyzed. We suppose that thermal damage is the major cause of tissue necrosis; however other factors causing necrosis such as direct tissue injury or perfusion deficits may interfere non-systematically with our analysis. It is a restriction of data analysis that the person who performed the segmentation knew the temperature maps and the coagulation zones; the study was thus not blinded. A general problem is the limited validity of specificity and negative predictive value; both depend on the portion of non-coagulated liver surface included in the concerned slices and vary therefore with the slice orientation, liver size and location of the tumour within the liver.

In conclusion, the presented data show that the size and localisation of the developing coagulation zone can be predicted by a binomial readout of the singular temperature maps at the end of energy application. The choice of the temperature cut-off level determines the accuracy of the predicted coagulation zone. Cut-off levels between 50°C and 55°C seem to overestimate the developing coagulation zone which may indicate a cellular protective mechanism. The 60°C cut-off level achieved the best prediction of the coagulation zone among the tested levels.

Acknowledgements The authors wish to thank Li Pan from Siemens Research for the development and provision of real-time MR sequences for applicator placements. J.R. and A.K. are employees of Siemens Healthcare (Germany).

References

1. Kudo M (2010) Radiofrequency ablation for hepatocellular carcinoma: updated review in 2010. *Oncology* 78(Suppl 1):113–124
2. Orlando A, Leandro G, Olivo M et al (2009) Radiofrequency thermal ablation vs. percutaneous ethanol injection for small hepatocellular carcinoma in cirrhosis: meta-analysis of randomized controlled trials. *Am J Gastroenterol* 104:514–524
3. Goldberg SN, Dupuy DE (2001) Image-guided radiofrequency tumor ablation: challenges and opportunities—part I. *J Vasc Intervent Radiol* 12:1021–1032
4. Lencioni R, Crocetti L, Cioni D et al (2004) Percutaneous radiofrequency ablation of hepatic colorectal metastases: technique, indications, results, and new promises. *Invest Radiol* 39:689–697
5. Livraghi T, Solbiati L, Meloni MF et al (2003) Treatment of focal liver tumors with percutaneous radio-frequency ablation: complications encountered in a multicenter study. *Radiology* 226:441–451
6. Ayav A, Germain A, Marchal F et al (2010) Radiofrequency ablation of unresectable liver tumors: factors associated with incomplete ablation or local recurrence. *Am J Surg* 200:435–439
7. Mulier S, Ruers T, Jamart J et al (2008) Radiofrequency ablation versus resection for resectable colorectal liver metastases: time for a randomized trial? An update. *Dig Surg* 25:445–460
8. Mulier S, Ni Y, Jamart J et al (2005) Local recurrence after hepatic radiofrequency coagulation: multivariate meta-analysis and review of contributing factors. *Ann Surg* 242:158–171
9. Pereira PL, Trubenbach J, Schenk M et al (2004) Radiofrequency ablation: in vivo comparison of four commercially available devices in pig livers. *Radiology* 232:482–490
10. Leyendecker JR, Dodd GD 3rd, Halff GA et al (2002) Sonographically observed echogenic response during intraoperative radiofrequency ablation of cirrhotic livers: pathologic correlation. *AJR Am J Roentgenol* 178:1147–1151
11. De Senneville BD, Mougnot C, Quesnon B et al (2007) MR thermometry for monitoring tumor ablation. *Eur Radiol* 17:2401–2410
12. Sapareto SA, Dewey WC (1984) Thermal dose determination in cancer therapy. *Int J Radiat Oncol Biol Phys* 10:787–800
13. Kickhefel A, Rosenberg C, Weiss CR et al (2011) Clinical evaluation of MR temperature monitoring of laser-induced thermotherapy in human liver using the proton-resonance-frequency method and predictive models of cell death. *J Magn Reson Imaging* 33:704–712

14. Rempp H, Clasen S, Boss A et al (2009) Prediction of cell necrosis with sequential temperature mapping after radiofrequency ablation. *J Magn Reson Imaging* 30:631–639
15. Hindmann JC (1966) Proton resonance shift of water in the gas and liquid state. *J Chem Phys* 44:4582–4592
16. Cernicanu A, Lepetit-Coiffe M, Roland J et al (2008) Validation of fast MR thermometry at 1.5 T with gradient-echo echo planar imaging sequences: phantom and clinical feasibility studies. *NMR Biomed* 21:849–858
17. Lepetit-Coiffe M, Laumonier H, Seror O et al (2010) Real-time monitoring of radiofrequency ablation of liver tumors using thermal-dose calculation by MR temperature imaging: initial results in nine patients, including follow-up. *Eur Radiol* 20:193–201
18. Schraml C, Schwenzer NF, Martirosian P et al (2009) Diffusion-weighted MRI of advanced hepatocellular carcinoma during sorafenib treatment: initial results. *AJR Am J Roentgenol* 193: W301–W307
19. Kierans AS, Elazzazi M, Braga L et al (2010) Thermoablative treatments for malignant liver lesions: 10-year experience of MRI appearances of treatment response. *AJR Am J Roentgenol* 194:523–529
20. Vigen KK, Daniel BL, Pauly JM et al (2003) Triggered, navigated, multi-baseline method for proton resonance frequency temperature mapping with respiratory motion. *Magn Reson Med* 50:1003–1010
21. De Senneville BD, Mougenot C, Moonen CT (2007) Real-time adaptive methods for treatment of mobile organs by MRI-controlled high-intensity focused ultrasound. *Magn Reson Imaging* 57:319–330
22. Terraz S, Cernicanu A, Lepetit-Coiffe M et al (2010) Radiofrequency ablation of small liver malignancies under magnetic resonance guidance: progress in targeting and preliminary observations with temperature monitoring. *Eur Radiol* 20:886–897
23. Peters RD, Chan E, Trachtenberg J et al (2000) Magnetic resonance thermometry for predicting thermal damage: An application of interstitial laser coagulation in an in vivo canine prostate model. *Magn Reson Med* 44:873–883
24. McDannold N, Jolesz F (2000) Magnetic resonance image-guided thermal ablations. *Top Magn Reson Imaging* 11:191–202
25. Chen L, Wansapura JP, Heit G et al (2002) Study of laser ablation in the in vivo rabbit brain with MR thermometry. *J Magn Reson Imaging* 16:147–152
26. Roujol S, Ries M, Quesson B et al (2010) Real-time MR-thermometry and dosimetry for interventional guidance on abdominal organs. *Magn Reson Med* 63:1080–1087
27. Haen SP, Gouttefangeas C, Schmidt D, et al. (2011) Elevated serum levels of heat shock protein 70 can be detected after radiofrequency ablation. *Cell Stress Chaperones*
28. Barnes JA, Dix DJ, Collins BW et al (2001) Expression of inducible Hsp70 enhances the proliferation of MCF-7 breast cancer cells and protects against the cytotoxic effects of hyperthermia. *Cell Stress Chaperones* 6:316–325
29. Lazebnik RS, Breen MS, Fitzmaurice M et al (2003) Radiofrequency-induced thermal lesions: subacute magnetic resonance appearance and histological correlation. *J Magn Reson Imaging* 18:487–495
30. Tsuda M, Rikimaru H, Majima K et al (2003) Time-related changes of radiofrequency ablation lesion in the normal rabbit liver: findings of magnetic resonance imaging and histopathology. *Invest Radiol* 38:525–531
31. Sequeiros RB, Kariniemi J, Ojala R et al (2010) Liver tumor laser ablation—increase in the subacute ablation lesion volume detected with post procedural MRI. *Acta Radiol* 51:505–511